HOKKAIDO UNIVERSITY

Title	Efficacy Assessment of Wide-Gap Torque-Type Rheometer for Evaluating Shear-Rate-Dependent Viscosity of Rice Porridge
Author(s)	Ohie, Kohei; Tasaka, Yuji
Citation	Journal of Texture Studies, 56(3), e70024 https://doi.org/10.1111/jtxs.70024
Issue Date	2025-06
Doc URL	https://hdl.handle.net/2115/97856
Rights	This is the peer reviewed version of the following article: Ohie, K. and Tasaka, Y. (2025), Efficacy Assessment of Wide-Gap Torque-Type Rheometer for Evaluating Shear-Rate-Dependent Viscosity of Rice Porridge. J Texture Stud, 56: e70024, which has been published in final form at https://doi.org/10.1111/jtxs.70024. This article may be used for non-commercial purposes in accordance with Wiley Terms and Conditions for Use of Self-Archived Versions. This article may not be enhanced, enriched or otherwise transformed into a derivative work, without express permission from Wiley or by statutory rights under applicable legislation. Copyright notices must not be removed, obscured or modified. The article must be linked to Wiley's version of record on Wiley Online Library and any embedding, framing or otherwise making available the article or pages thereof by third parties from platforms, services and websites other than Wiley Online Library must be prohibited.
Type	journal article
File Information	Manuscript.pdf

Hokkaido University Collection of Scholarly and Academic Papers : HUSCAP

RESEARCH ARTICLE

Efficacy assessment of wide-gap torque-type rheometer for evaluating shear-rate-dependent viscosity of rice porridge

Kohei Ohie[1] and Yuji Tasaka[1]

[1] Laboratory for Flow Control, Faculty of Engineering, Hokkaido University, Sapporo 060-8628, Japan

Correspondence

Kohei Ohie, Laboratory for Flow Control, Faculty of Engineering, Hokkaido University, Sapporo 060-8628, Japan
Email: koheiohie@gmail.com

Funding information

JSPS KAKENHI (Grant No. 22J20991), Creative Research Institution of Hokkaido University, The Public Foundation of Elizabeth Arnold-Fuji

Abbreviations: VPAR, velocity-profiling-assisted rheometry; CMC, carboxymethyl cellulose.

Abstract

Rheological property is a key factor not only in how consumers choose and enjoy foods, but also in ensuring the safe eating and swallowing for dysphagia patients. The rheological measurements of fluid foods containing millimeter-sized ingredients, however, have been still challenging due to the limitations of a standard torque-type rheometer. We herein examine the efficacy of a wide-gap torque-type rheometer for evaluating shear-rate-dependent viscosity of heterogeneous fluid foods containing millimeter-sized ingredients. In addition to numerical validation using a shear-thinning fluid obeying the power law model, the apparent flow curves of silicone oil and carboxymethyl cellulose aqueous solution were compared with those obtained by the standard rheometer. It was also confirmed that the shear-thinning properties of plain, egg, and bean porridge well match those identified by the recently developed velocity-profiling-assisted rheometry. These results reinforce the wide-gap torque-type rheometer to be practical for probing the rheology of the complex fluid foods.

Keywords

rheometry, heterogeneous fluids, rice porridge, polymer, oil

1 INTRODUCTION

Food texture is a key factor in how consumers choose and enjoy food products. Rheological properties representing the texture by, for example, viscosity are not only perceived in non-oral process such as mixing and pouring a fluid food with a spoon, but also in oral process such as compressing a bolus between tongue and plate and swallowing it [1]. Rheological properties also play an important role to assure the safe eating and swallowing process, as the recent population aging has led a rapid increase in the number of dysphagia patients [2, 3]. In order to elucidate the causal relationship between the swallowing process and the rheological properties, ultimately to prepare optimal fluid foods that prevent aspiration, both in vivo and in vitro measurements have been performed in the swallowing medical field. In aspect of the in vivo measurements, commonly used methods include videofluorography, videoendoscopic evaluation, and ultrasonic Doppler velocimetry for observing the bolus behavior from the nasopharynx to the hypopharynx [4-9]. Regarding the in vitro measurements, a standard torque-type rheometer is often used to characterize shear-rate-dependent viscosity. Based on both in vivo and in vitro measurements, it is known that the fluids with relatively high shear-thinning are more suitable for successful swallowing [10-11]. It is turned out recently that elongational viscosity and yield stress are also important in the dynamics of food bolus [12-15].

The standard torque-type rheometer offers a variety of geometry options, including plate-plate, cone-plate, and double concentric cylinders. The common principle of the rheometer is that a test fluid is filled in a sub-millimeter gap for assuring a constant shear rate applied to the test fluid in the gap [16]. The shear stress and shear rate are indirectly evaluated by measuring the axial torque and rotation speed of the rod. For assuring the homogeneity of the test fluid in the gap, the dispersion size has to be less than one tenth of the gap size [17-19], and hence the bulk-averaged viscosity as apparent viscosity can be measured. However, most fluid foods, such as rice porridge and yogurt with fruit pulps, are spatially heterogeneous containing millimeter-sized ingredients from a viewpoint of the gap size of the standard rheometer. Yoshida et al. daringly measured gelled dessert containing fruit pulps by a standard torque-type rheometer with a plate-plate geometry, and confirmed puzzling results where the shear stress oscillates as the shear rate increases [20]. Ohie et al. measured suspensions of solid spherical particles dispersed in silicone oil by the standard torque-type rheometer with a plate-plate geometry. The diameter of the particles is in several $100\ \mu$m, and the effective viscosity was overestimated in comparison with the theory [21]. The measurement of these heterogeneous fluids has been challenging in the field of rheology.

For measuring the heterogeneous fluid foods containing millimeter-sized ingredients, there are some complementary methods such as ball measuring system [22, 23], single cylinder rotational viscometer (Brookfield viscometer) [24], and falling sphere viscometry. Schatzmann et al. developed a ball measuring system for fluids with particle sizes up to 10 mm [22]. The system consists of a round container, into which a test fluid is filled, and a sphere is eccentrically rotated in the fluid. By measuring both angular velocity and axial torque, the apparent shear rate and shear stress are evaluated. The Brookfield viscometer consists of double concentric cylinders, and the inner cylinder is rotated with a constant speed. Both the angular velocity and axial torque are measured, and these are converted into the apparent shear rate and shear stress. The apparent flow curve can be obtained by gradually increasing the rotation speed of the inner cylinder. The gap size is relatively wider than those of standard torque-type rheometers, it is therefore applicable for measuring spatially heterogeneous fluids such as aqueous powder slurries [24-26]. In the falling sphere viscometry, a sphere is dropped into a test fluid, and its terminal velocity is measured. In a case of Newtonian fluids, the terminal velocity is inversely proportional to the viscosity in a laminar flow [27, 28]. The falling sphere viscometer utilizes this relationship for evaluating the apparent viscosity of non-Newtonian fluids, and has been utilized to bubble suspensions and solid-liquid multi-phase fluids [29, 30]. These methods are facile and practical for evaluating the apparent rheological properties and relative evaluation of multiple samples. The rheometers introduced above were all designed with gap sizes or tank sizes sufficiently larger than the dispersed particles to ensure that fluid foods could be regarded as continuous body at that scale. However, the theoretical framework used to evaluate the rheological properties from the controlled rotational speed and the measured axial torque assumes a Newtonian fluid. This framework is then directly applied to non-Newtonian fluids. Consequently, the extent to which these rheometers accurately assess the non-Newtonian behavior of fluid foods has not been thoroughly validated, which serves as a major motivation for this research. Although there are some previous work comparing the Brookfield viscometer with a standard torque-type rheometer and also investigating effects of the geometry [24, 31, 32], efficacy of the wide-gap torque-type rheometer for evaluating heterogeneous fluids is still unclear due to the lack of reliable measurement methods to be referenced with.

For accurately evaluating these heterogeneous fluids, velocity-profiling-assisted rheometry (VPAR) was developed [33-37]. The usual experimental setup consists of double concentric cylinders, where the outer cylinder is rotated with a constant angular velocity and the inner cylinder is fixed to an axial torque sensor for measuring the wall shear stress. There is a one-directional azimuthal shear flow realized, and the resulting non-linear velocity profile is measured by ultrasonic velocity profiling [38-40]. The shear rate profile is obtained by spatial derivative of the velocity profile. The stress profile is obtained from the Cauchy's equation of motion, that is, conservation of angular momentum by substituting the measured wall shear stress. The measurement examples are emulsions [33, 34], carbopol microgels [35], concentrated pulp fiber suspensions [36], and wormlike micellar solutions [37]. Recently, Ohie et al. [41] improved the experimental setup of VPAR for more accurate rheological evaluation. They applied it for measuring rice porridge, which contains millimeter-sized rice grains. With the obtained flow curve, they predicted pipe flows and the velocity profiles were in good agreement with those measured in a pilot pipeline system. Ohie et al. [42] further measured plain, egg, and bean porridge, and it was revealed that the flow curves of rice porridge are well characterized by the power low model. Using the rheology data, they showed that the spreading behavior on a horizontal plane and descending flow after a contraction part on an inclined plane, which are fundamental flows in the eating and swallowing process, are well rationalized by the rheology data. VPAR is thus a promising method for measuring rheology of fluid foods containing millimeter-sized ingredients. However, as VPAR is used in combination with velocity profile measurement such as the ultrasonic velocity profiling or high-speed camera [43], it is more expensive to implement than the wide-gap torque-type rheometer, and requires technical knowledge and experience. Cost effectiveness is a key factor required for rheometry to be widely applied in many fields such as not only food, but also chemical, civil and geological science fields. In addition, the ultrasonic velocity profiling has weaknesses such as difficulty in measuring highly concentrated suspensions due to the attenuation of the ultrasonic waves [21, 44].

In this paper, we revisit the wide-gap torque-type rheometer and examine its efficacy for evaluating shear-rate-dependent viscosity of the heterogeneous fluids. The recent development of VPAR has made it possible to measure the rheology of complex fluids, which provides reliable reference data to verify the wide-gap torque-type rheometer to the heterogeneous fluids. In the following Sec. 2, theoretical background of the wide-gap torque-type rheometer is denoted. The validity of the rheometer is examined in both numerical and experimental aspects. As most of the fluid foods have shear-thinning properties following the power law model, the axial torque of the shear-thinning fluid is theoretically derived and the analytical procedure of the rheometry is demonstrated in Sec. 3. The evaluated rheological parameters are compared with the original values. In Sec. 4, the experimental validation is conducted using silicone oil, carboxymethyl cellulose aqueous solution, and rice porridge, which are typical Newtonian, shear-thinning, and spatially heterogeneous non-Newtonian fluids, respectively. Limitations of the rheometer are summarized in Sec. 5, and summary is finally given in Sec. 6.

2 WIDE-GAP TORQUE-TYPE RHEOMETER

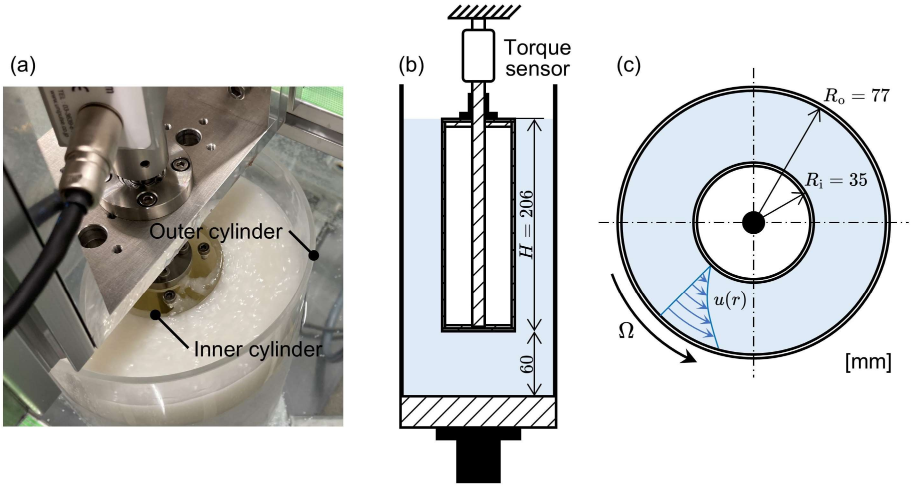

FIGURE 1 Experimental setup of the wide-gap torque-type rheometer: (a) photograph of the setup taken from the top, where the plain porridge is filled between the double concentric cylinders, (b) schematic of the vertical cross-sectional view, and (c) schematic of the horizontal cross-sectional view.

Theoretical background of the rheometry is described here. The experimental setup is shown in Fig. 1. The outer cylinder with the radius of $R_o = 77$ mm is rotated by a stepping motor. At an angular rotation speed of Ω, the azimuthal wall velocity is $U_{wall} = R_o\Omega$. The inner cylinder with the radius of $R_i = 50$ mm and the height of $H = 206$ mm is connected to an axial torque sensor (UTM III, 0.5 Nm, Unipulse Co., Ltd., Japan). One-directional azimuthal flow is induced between the double concentric cylinders. In this steady flow, the shear stress satisfies the Cauchy's equation of motion [45],

$$\frac{d\tau}{dr} + \frac{2\tau}{r} = 0. \tag{1}$$

Assuming a Newtonian fluid with the viscosity coefficient of μ, the shear stress is given as $\tau = \mu\dot{\gamma}$, where $\dot{\gamma}$ is the shear rate defined as [45]

$$\dot{\gamma}(r) = \frac{du}{dr} - \frac{u}{r}. \tag{2}$$

The Newtonian fluid therefore satisfies the following equation,

$$\frac{d^2u}{dr^2} + \frac{1}{r}\frac{du}{dr} - \frac{u}{r^2} = 0. \tag{3}$$

Non-slip conditions are assumed to be satisfied on the inner and outer cylinder surfaces, that is, $u = 0$ at $r = R_i$ and $u = U_{wall}$ at $r = R_o$. With these boundary conditions, the velocity profile is derived as

$$u(r) = \frac{U_{wall}}{R_o/R_i - R_i/R_o}\left(\frac{r}{R_i} - \frac{R_i}{r}\right). \tag{4}$$

Substituting this velocity profile into Eq. 2, the shear rate profile is

$$\dot{\gamma}(r) = \frac{2R_\mathrm{i}R_\mathrm{o}\Omega}{(R_\mathrm{o}/R_\mathrm{i} - R_\mathrm{i}/R_\mathrm{o})r^2}. \tag{5}$$

The bulk-averaged shear rate is here defined as

$$\bar{\dot{\gamma}}(\Omega) = \frac{1}{\pi(R_\mathrm{o}^2 - R_\mathrm{i}^2)}\int_{R_\mathrm{i}}^{R_\mathrm{o}} 2\pi r\dot{\gamma}dr = \frac{4R_\mathrm{i}^2R_\mathrm{o}^2\Omega}{(R_\mathrm{o}^2 - R_\mathrm{i}^2)^2}\ln\left(\frac{R_\mathrm{o}}{R_\mathrm{i}}\right). \tag{6}$$

The shear stress profile is derived from Eq. 1 as

$$\tau(r) = \tau_\mathrm{wall}\left(\frac{R_\mathrm{i}}{r}\right)^2, \tag{7}$$

where τ_wall is the wall shear stress acting on the inner cylinder surface given as $\tau_\mathrm{wall} = \mu\dot{\gamma}(r = R_\mathrm{i})$. The bulk-averaged shear stress is here defined as

$$\bar{\tau}(\Omega) = \frac{1}{\pi(R_\mathrm{o}^2 - R_\mathrm{i}^2)}\int_{R_\mathrm{i}}^{R_\mathrm{o}} 2\pi r\tau dr = \frac{T}{k\pi(R_\mathrm{o}^2 - R_\mathrm{i}^2)H}\ln\left(\frac{R_\mathrm{o}}{R_\mathrm{i}}\right). \tag{8}$$

where T is the axial torque acting on the inner cylinder, $T = 2\pi R_\mathrm{i}^2 H\tau_\mathrm{wall}$. The correction factor k is for taking the additional axial torque induced by the shear acting on the bottom of the inner cylinder into account. Assuming infinite height of the inner cylinder gives $k = 1$, and usually $k > 1$ for finite cylinder height. Fundamentally, this additional torque becomes negligible if the distance between the bottom surfaces of the inner and outer cylinders is sufficiently large [42]. With Eqs. 6 and 8, the flow curve $\bar{\tau}(\bar{\dot{\gamma}})$ is obtained by controlling the angular rotation speed Ω and measuring the corresponding axial torque T. Even in the case of non-Newtonian fluids, the wide-gap torque-type rhometry evaluates the apparent flow curve based on Eqs. 6 and 8 by gradually varying Ω and measuring the corresponding T.

3 NUMERICAL VALIDATION

Despite doubtless derivation of the apparent flow curve in Sec. 2, it is still unclear how accurately the apparent flow curve reflects non-Newtonian properties. Efficacy assessment of the wide-gap torque-type rheometer for evaluating shear-rate-dependent viscosity is examined in both numerical and experimental aspects. The numerical validation is first examined. As a representative rheology model for characterizing fluid foods, a shear-thinning fluid following the power law model is used here. The model describes the shear stress and the shear rate as

$$\tau = K\dot{\gamma}^n, \tag{9}$$

where K is the consistency, and n is the power law exponent. For a Newtonian fluid, $n = 1$, shear-thinning property appears as n decreases, and shear-thickening property is intensified as n increases beyond unity. For a certain combination of K and n, the exact velocity profile can be derived, and the wall shear stress on the inner cylinder surface is obtained as well as the shear stress profile between the double concentric cylinders. From the standpoint of the wide-gap torque-type rheometer, only the angular rotation speed Ω and the axial torque T are measured, and the apparent flow curve is evaluated from Eqs. 6 and 8 with Ω and T. Herein, it is examined how the apparent flow curve can capture the original parameters, K and n.

The velocity profile is first derived mathematically. Substituting the power law model (Eq. 9) into the Cauchy's equation of motion (Eq. 1), it is transformed to

$$\frac{d^2u}{dr^2} + \alpha\frac{1}{r}\frac{du}{dr} - \alpha\frac{u}{r^2} = 0, \tag{10}$$

with $\alpha = 2/n - 1$. Non-slip conditions are assumed on the inner and outer cylinder surfaces, that

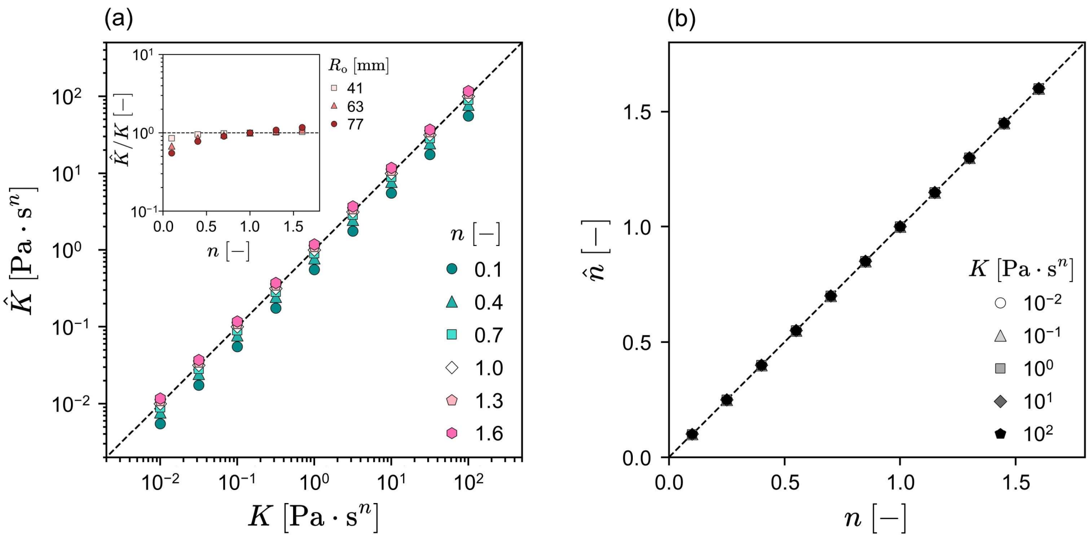

FIGURE 2 Numerical validation of the wide-gap torque-type rheometry: (a) the consistency $\widehat{K}$ evaluated from the apparent flow curves obtained by the wide-gap torque-type rheometry in comparison with the original consistency K, and (b) the power law exponent $\hat{n}$ evaluated from the apparent flow curves in comparison with the original power law exponent n. The dashed lines show where $\widehat{K} = K$ and $\hat{n} = n$. The graph dawn inside Fig. 2(a) shows the ratio, $\widehat{K}/K$, under different n and the radius of the outer cylinder, R_o.

is, $u = 0$ at $r = R_i$ and $u = U_{wall}$ at $r = R_o$, the velocity profile is derived as

$$u(r) = \frac{U_{wall}}{R_o/R_i^\alpha - R_i/R_o^\alpha}\left(\frac{r}{R_i^\alpha} - \frac{R_i}{r^\alpha}\right). \quad (11)$$

The derivation of velocity distributions for fluids following the power-law model, although for a different type of flow, has been analytically conducted previously for the axial flow within a pipe [46, 47], where the resulting velocity distribution is similar in form to Eq. 11. Substituting this velocity profile Eq, 11 into Eq. 2, the shear rate profile is

$$\dot{\gamma}(r) = \frac{(\alpha+1)R_i R_o \Omega}{(R_o/R_i^\alpha - R_i/R_o^\alpha)r^{\alpha+1}}. \quad (12)$$

The wall shear stress is $\tau_{wall} = K|\dot{\gamma}(r = R_i)|^n$, and the axial torque is derived as

$$T = 2\pi R_i^2 HK\left[\frac{(\alpha+1)\Omega}{1-(R_i/R_o)^{\alpha+1}}\right]^n. \quad (13)$$

From the standpoint of the wide-gap torque-type rheometry, the angular rotation speed Ω is increased from 0 rpm to 60 rpm by 1 rpm increment, the corresponding axial torque is calculated by Eq. 13, and the apparent flow curve is obtained by Eqs. 6 and 8. The consistency K and the power law exponent n are varied from 10^{-2} Pa s^n to 10^2 Pa s^n, and from 0.1 to 1.6, respectively. All the apparent flow curves are confirmed to be linear in the log-log scale (not shown in figures), and fitted with the following power law function,

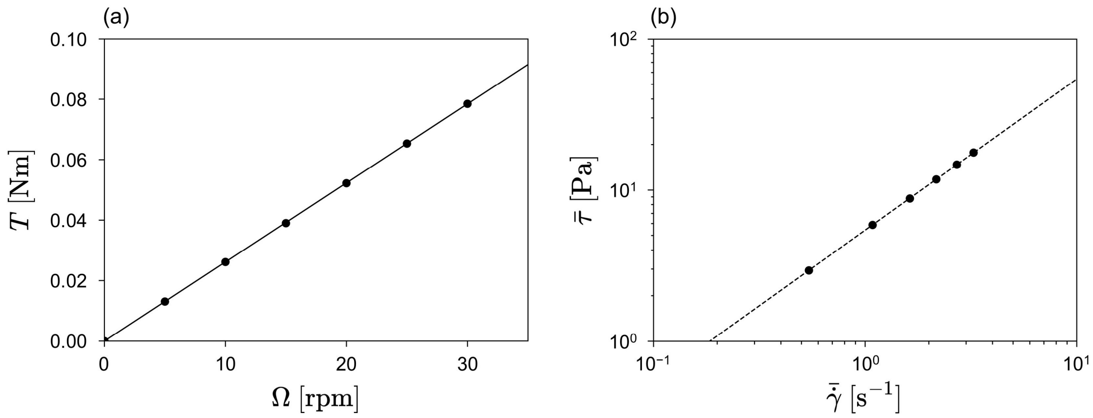

FIGURE 3 Measurement results of the silicone oil: (a) Time-averaged axial torque T as a function of the angular rotation speed of the outer cylinder Ω, and (b) flow curve evaluated from T and Ω with Eqs. 6 and 8. The solid line in the left figure shows the linear fitting result based on the least squares method. The dashed line in the right figure shows the flow curve of the viscosity coefficient of 5.41 Pa s measured by a standard torque-type rheometer.

$$\bar{\tau} = \hat{K}\bar{\dot{\gamma}}^{\hat{n}}. \tag{14}$$

The obtained parameters $\hat{K}$ and $\hat{n}$ determined based on the least squares method are summarized in Fig. 2 in comparison with the original parameters, K and n. The dashed lines show where exactly $\hat{K} = K$ and $\hat{n} = n$. All the plots are closely arranged on the diagonal lines, particularly, $\hat{n}$ perfectly matches the original n independent of the set value of K. Regarding the consistency $\hat{K}$, it is underestimated in comparison with the original K as the degree of shear thinning increases. At $n = 0.1$, the consistency is evaluated at about half of the original value as $\hat{K}/K = 0.55$ (see the graph drawn inside Fig. 2(a)). This deviation is suppressed as the radius of the outer cylinder decreases, that is, the gap size becomes narrower. The gap size is generally required to be at least ten times larger than the dispersion [17-19]. The numerical experiment here shows that shear-thinning property can be more accurately captured by reducing the gap size as much as possible while satisfying this requirement.

4 EXPERIMENTAL VALIDATION

In experimental aspect, three kinds of test fluids are examined. The first one is silicone oil, a typical Newtonian fluid. The viscosity evaluated by the wide-gap torque-type rheometer is compared with the catalog value of the silicone oil in Sec. 4.1. The second one is carboxymethyl cellulose (CMC) aqueous solution, a typical shear-thinning fluid. The measurement result is compared with a standard torque-type rheometer with a cone-plate geometry. Applicability of the wide-gap torque-type rheometer to evaluate homogeneous shear-thinning fluid is experimentally examined in Sec. 4.2. The last one is rice porridge. Three kinds of porridge are examined; plain, egg, and bean porridge. They contain rice grains, egg flowers, and red beans, which are millimeter-sized dispersions. The measured flow curves are compared with the recently developed velocity-profiling-assisted rheometry (VPAR) [41, 42]. The efficacy assessment of the wide-gap torque-type rheometer for evaluating shear-rate-dependent viscosity of the heterogeneous fluids is discussed in Sec. 4.3.

4.1 Silicone oil

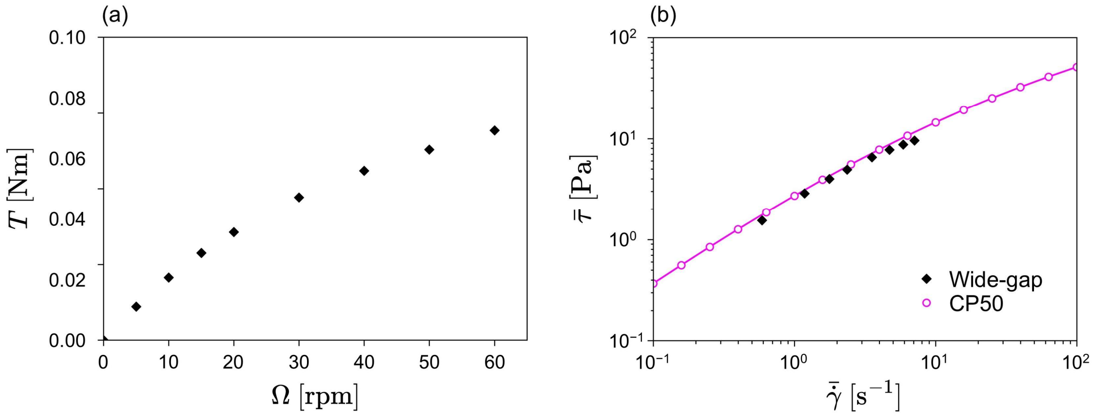

FIGURE 4 Measurement results of the carboxymethyl cellulose (CMC) aqueous solution: (a) Time-averaged axial torque T as a function of the angular rotation speed of the outer cylinder Ω, and (b) flow curve evaluated from T and Ω with Eqs. 6 and 8. The diamond and circles show the flow curves evaluated by the wide-gap torque-type rheometer and a standard torque-type rheometer with a cone-plate geometry. To facilitate comparison between the results obtained with the standard torque-type rheometer (CP50) and those from the wide-gap torque-type rheometer, the CP50 data points have been connected by solid lines.

A silicone oil (KF-96-5,000cs, Shin-Etsu Chemical Co., Ltd., Japan) was filled in the gap of the experimental setup as shown in Fig. 1. The original data of the silicone oil is from the previous research [19]. The kinematic viscosity is 5000 mm^2/s at 25°C and the density is 972 kg/m^3. The experiment was conducted at 20°C. The angular rotation speed of the outer cylinder was increased from $\Omega = 0$ rpm to 30 rpm by 5 rpm increment. For each rotational speed condition, the measurement duration was 30 s. Additionally, to ensure that the flow within the gap reached equilibrium, an interval of 60 s was set before each measurement. Defining that the characteristic length scale as L and the characteristic kinematic viscosity as ν, the viscous diffusion time is estimated as L^2/ν. Given that the outer cylinder radius is $R_{\mathrm{out}} = 77$ mm and the inner cylinder radius is $R_{in} = 35$ mm, the characteristic length scale is $L = R_{\mathrm{out}} - R_{\mathrm{in}} = 42$ mm. Assuming a conservatively low estimation for the kinematic viscosity also considering the CMC solution and rice porridge denoted later, $\nu = 10^3$ mm^2/s, the viscous diffusion time is on the order of $O(1)$ s. Thus, the interval set mentioned above is considered sufficient. The time-averaged axial torque is shown in Fig. 3(a). The toque is confirmed to linearly increase asΩ increases. The solid line in Fig. 3(a) is the linear fitting result based on the least squares method. The gradient is evaluated to be $dT/d\Omega = 2.6 \times 10^{-3}$ Nm/rpm . Assuming $k = 1$ tentatively, the corresponding viscosity is 6.24 Pa s. The viscosity coefficient evaluated by a standard torque-type rheometer (MCR702e, Anton-Paar, Austria) with a cone-plate geometry is 5.41 Pa s. The correction factor k is therefore $k = 1.15$ in this experimental setup. Regarding the measurement by the standard torque-type rheometer, the diameter of the cone-shaped fixture used was 50 mm, with an angle of 1°. Additionally, multiple measurements under identical conditions were conducted, and all the resulting flow curves overlapped, suggesting that the precision is sufficient for comparison with the wide-gap torque-type rheometer. The axial torque and the angular rotation speed measured in the experimental setup are then converted to the bulk-averaged shear stress $\bar{\tau}$ and shear rate $\bar{\dot{\gamma}}$ as shown in Fig. 3(b). The dashed line behind the plots is the flow curve with the viscosity coefficient of 5.41 Pa s. The flow curve evaluated by the wide-gap torque-type rheometer is confirmed to match the reference line.

4.2 Carboxymethyl cellulose solution

A carboxymethyl cellulose (CMC) aqueous solution is well known to exhibit shear-thinning

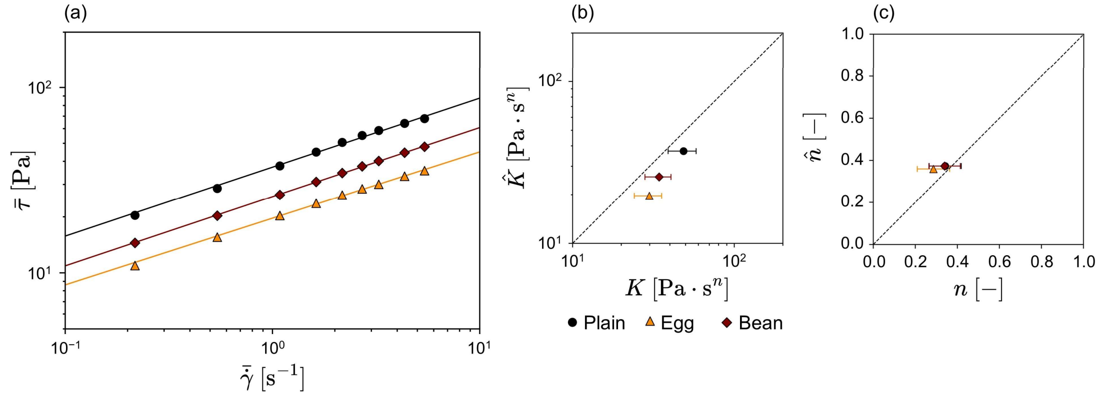

FIGURE 5 Measurement results of the rice porridge: (a) Bulk-averaged shear stress $\bar{\tau}$ as a function of the bulk-averaged shear rate $\bar{\dot{\gamma}}$, (b) and (c) comparison of the consistency $\hat{K}$ and the power law exponent $\hat{n}$ determined from the flow curves in comparison with K and n determined from those evaluated by VPAR. The shape of the symbols corresponds to the porridge type. The solid lines in the left figure show the power law fitting results based on the least squares method. The dashed lines in the middle and right figures show where $\hat{K} = K$ and $\hat{n} = n$. The horizontal error bars indicate three times the standard deviations in the VPAR evaluation.

viscosity [48, 49]. The CMC used in this experiment (CMC1190, Daicel Miraizu Ltd., Japan) has the weight-averaged molecular weight of 8.2×10^5 g/mol. The degree of etherification is 0.63 and the sodium chloride content is 0.14%. The CMC powder was added to pure water so that the concentration becomes 1.2 wt.% the day before the experiment and stirred overnight using an impeller. During the experiment with the CMC solution, due to laboratory circumstances, the experimental setup shown in Fig. 1 was not available, different double concentric cylinders was instead used, where the radii of the inner and outer cylinders are $R_{\mathrm{i}} = 50\ \mathrm{mm}$ and $R_{\mathrm{o}} = 105\ \mathrm{mm}$, and the height of the inner cylinder is $H = 160\ \mathrm{mm}$. This experimental setup is specifically explained elsewhere [21]. What is essentially different from the setup in Fig. 1 is that a stepped disk is independently installed closely below the inner cylinder to suppress the shear applied to the bottom of the inner cylinder, hence the correlation coefficient is $k = 1$. The measurement was conducted under the temperature of 25°C.

The angular rotation speed of the outer cylinder was increased from $\Omega = 0\ \mathrm{rpm}$ to 20 rpm by 5 rpm inclement, and from $\Omega = 20\ \mathrm{rpm}$ to 60 rpm by 10 rpm inclement. The time-averaged axial torque is shown in Fig. 4(a). In contrast to the silicone oil, T increases with the gradient decreasing. These are converted to the flow curve as shown in Fig. 4(b). The diamond symbols show the results obtained by the wide-gap torque-type rheometer. The gradient is smaller than the unity in the log-log scale, the CMC therefore has a shear-thinning property. The circles behind are the results of the same sample measured by the standard torque-type rheometer with the cone-plate geometry (CP50) also used for the silicon oil in Sec. 4-2. The stress evaluated by the wide-gap torque-type rheometer is slightly lower than that evaluated by the torque-type rheometer, but totally the shear-thinning property is confirmed to be well captured. This result experimentally reinforces the validity of the wide-gap torque-type rheometer for evaluating the shear-rate-dependent viscosity even in fluids that do not perfectly obey power law model.

4.3 Rice porridge

Three kinds of commercial rice porridge (Ajinomoto Co., Inc., Japan) are examined. The plain porridge is the most standard type and it contains oval-shaped millimeter-sized rice grains. The second one is egg porridge, which contains not only rice grains but also egg flowers. The last one is bean porridge, which contains red beans as ingredients with a volume fraction of several percent. The porridge was filled in the experimental setup as shown in Fig. 1(a) with the temperature kept at 25ºC. The outer cylinder was rotated from $\Omega = 2$ rpm, 5 rpm to 30 rpm by 5 rpm increment, and from $\Omega = 30$ rpm to 50 rpm by 10 rpm increment. The flow curves of the porridge evaluated by the wide-gap torque-type rheometer are shown in Fig. 5(a). The correction factor $k = 1.15$ identified in Sec. 4.1 was used for the analysis. The solid lines show the power law fitting results based on the least squares method. The flow curves of the porridge are confirmed to follow the power law model. The plain porridge is the most viscous, the bean porridge is the second, and the egg porridge has the lowest viscosity.

The same porridge was also measured by VPAR previously [42], and they were also well characterized by the power law model. The consistency $\widehat{K}$ and the power law exponent $\hat{n}$ identified from the flow curves in Fig. 5(a) with Eq. 14 are summarized in Fig. 5(b) and (c) in comparison with those obtained from the flow curves measured by VPAR, K and n. The solid lines indicate where $\widehat{K} = K$ and $\hat{n} = n$, and all the plots are confirmed to be closely arranged on these lines. The porridge has the shear-thinning property of $n = 0.3 - 0.4$, the consistency $\widehat{K}$ is evaluated to be smaller than K as described in Sec. 3. The maximum deviation is $\widehat{K}/K = 0.66$ in the egg porridge. This error may be not negligible when an objective of the rheological measurement is to accurately predict, for example, industrial pipeline flows, but it is considered to be within an acceptable range when an objective is to categorize fluid foods into several groups, for example into 3 or 4 groups regarding each K and n. When conducting rheological measurements of suspensions, it is crucial to address the spatial uniformity of the solid particle distribution. In the measurement by VPAR, it is generally possible to obtain a flow curve under a given condition of the outer cylinder's rotational speed Ω. This is because VPAR allows for a spatial distribution of shear rates within the gap and enables the local evaluation of shear stress at each radial position. In the previous study, VPAR was applied under different rotational speed Ω conditions and confirmed that the obtained multiple flow curves overlapped [42]. Consequently, this indicates the presence of a fluid with identical rheological properties across the radial direction, implying that the rice grains are uniformly dispersed within the gap. As the densities of the rice grains and the continuous phase are expected to differ slightly, prolonged measurements would likely cause the rice grains to move toward either the inner or outer cylinder due to additional forces even the densities are the same. However, as mentioned above, the rice grains are considered to be uniformly dispersed in the gap during the present measurements. This is likely because the starch solution, which serves as the continuous phase, exhibits extremely high viscosity, generating sufficient viscous stress to suppress the radial movement of the rice grains.

Finally, a brief discussion on the obtained rheological parameters is provided. The porridge can be regarded as a suspension in which rice grains, considered as ellipsoidal solid particles, are dispersed in a shear-thinning starch solution. In the present study, the degree of shear-thinning behavior of the porridge was evaluated approximately $n = 0.3 - 0.4$, which is significantly smaller than the value typically observed for starch solutions alone [50]. It is known that suspensions of dispersed ellipsoidal particles can exhibit additional shear-thinning behavior even when the continuous phase is a Newtonian fluid [51, 52]. The presence of dispersed rice grains is therefore considered to enhance the effective shear-thinning behavior synergistically with the inherent shear-thinning nature of the starch solution. There still remain many unresolved aspects regarding the suspension rheology of ellipsoidal particles in non-Newtonian fluids, making this an important future research direction.

5 LIMITATIONS OF THE RHEOMETRY

Limitations and precautions in use of the wide-gap torque-type rheometer are finally denoted in aspects of a slip property, dispersion size, and measurable range of the shear stress and shear rate. Regarding the slip property firstly, the non-slip boundary conditions are assumed in the derivation of Eq. 4. If a slip flow occurs on the inner or outer cylinder surface, the actual deformation applied to the test fluid is smaller than that estimated by Eq. 6, which leads to inaccuracy of the obtained apparent flow curve. Occurrence of wall slip causes a relative velocity between the cylinder surface and the test fluid around it, and it is relatively easy to know whether the slip occurs or not. For example, as the cylindrical vessel is made of acrylic resin, the porridge adhering to the wall can be observed from outside the cylinder. By making a point or a line on the outer cylinder wall in advance, it can be evaluated whether the relative motion occurs between the porridge and the outer cylinder wall when it is rotated. If the slip occurs, it is effective to make the cylinder surface rough as is often done in standard torque-type rheometers. Regarding the dispersion size, it needs to be one-tenth or less of the gap size in order to evaluate the effective viscosity of the test fluid as a bulk. If the dispersion size is larger than this limitation, the friction between the dispersion and the cylinder surface becomes dominant, and the abnormal viscosity is detected as is also observed in the measurement by a standard torque-type rheometer [20, 21]. Making the gap size too large, on the other hand, lead to uncertainty for evaluating a shear-thinning fluid, as pointed out in Sec. 3. It is therefore required to narrow the gap size while fully satisfying the one-tenth limitation. The gap size also affects the measurable range of the shear stress and shear rate. Assuming the minimum and maximum angular rotation speed of the outer cylinder are Ω_{min} and Ω_{max}, the measurable shear rate range is given as

$$\bar{\dot{\gamma}}_{\mathrm{min}} = \frac{4R_{\mathrm{i}}^2 R_{\mathrm{o}}^2 \Omega_{\mathrm{min}}}{(R_{\mathrm{o}}^2 - R_{\mathrm{i}}^2)^2} \ln\left(\frac{R_{\mathrm{o}}}{R_{\mathrm{i}}}\right), \tag{15}$$

$$\bar{\dot{\gamma}}_{\mathrm{max}} = \frac{4R_{\mathrm{i}}^2 R_{\mathrm{o}}^2 \Omega_{\mathrm{max}}}{(R_{\mathrm{o}}^2 - R_{\mathrm{i}}^2)^2} \ln\left(\frac{R_{\mathrm{o}}}{R_{\mathrm{i}}}\right). \tag{16}$$

Tentatively substituting $\Omega_{\mathrm{min}} = 2$ rpm and $\Omega_{\mathrm{min}} = 60$ rpm, which are determined by the spec of the stepping motor used in the current setup, the shear rate range is from $\bar{\dot{\gamma}}_{\mathrm{min}} = 0.2\ \mathrm{s}^{-1}$ to $\bar{\dot{\gamma}}_{\mathrm{max}} = 6.5\ \mathrm{s}^{-1}$. The range with this rheometry is at most one order of magnitude, which is much narrower than a standard torque-type rheometer. Note that the ratio of Eqs. 15 and 16 is $\Omega_{\mathrm{min}}/\Omega_{\mathrm{max}}$, which does not depend on the geometry. The range of the measurable shear rates is therefore determined by the minimum and maximum rotation speed of the motor. The measurable range of the shear stress is determined by the minimum torque T_{min} and the maximum torque T_{max} measured by the axial torque sensor,

$$\bar{\tau}_{\mathrm{min}} = \frac{T_{\mathrm{min}}}{\pi(R_{\mathrm{o}}^2 - R_{\mathrm{i}}^2)H} \ln\left(\frac{R_{\mathrm{o}}}{R_{\mathrm{i}}}\right), \tag{17}$$

$$\bar{\tau}_{\mathrm{max}} = \frac{T_{\mathrm{max}}}{\pi(R_{\mathrm{o}}^2 - R_{\mathrm{i}}^2)H} \ln\left(\frac{R_{\mathrm{o}}}{R_{\mathrm{i}}}\right). \tag{18}$$

Substituting $T_{\mathrm{min}} = 0.5 \times 10^{-4}$ Nm and $T_{\mathrm{max}} = 0.5$ Nm, which is determined by the spec of the torque sensor, the measurable shear stress range is from $\bar{\tau}_{\mathrm{min}} = 1.3 \times 10^{-2}$ Pa to $\bar{\tau}_{\mathrm{max}} = 1.3 \times 10^{2}$ Pa. The geometry and spec of the used torque sensor have to be chosen so that the measurable range of the shear stress and shear rate can cover the target measurement range. Finally, attention is also required regarding the correction factor k. In this study, it was determined using a Newtonian fluid, specifically silicone oil. In the analysis of the wide-gap torque-type rheometer, the velocity distribution within the gap is first derived under the assumption of a Newtonian fluid. The effective viscosity of a non-Newtonian fluid is then evaluated using the relationship between the controlled rotational speed and the measured axial torque as mentioned in Sec. 2. Therefore, the correction factor is strictly valid only for Newtonian fluids. Even considering this issue, Sec. 4.3 demonstrates that the wide-gap torque-type rheometer is effective in evaluating the shear-rate-dependent viscosity of fluid foods containing millimeter-sized ingredients. However, it is more effective to mount a stepped disk independent of the inner cylinder to block the shear flow propagating from the bottom surface of the outer cylinder to that of the inner cylinder [42], which was employed for the measurement of the CMC solution in Sec. 4.2.

6 SUMMARY

In this paper, efficacy of the wide-gap torque-type rheometer for evaluating shear-rate-dependent viscosity of heterogeneous fluid foods was examined in both numerical and experimental aspects. Based on the velocity profile of a Newtonian fluid in the double concentric cylinders, the bulk-averaged shear stress $\bar{\tau}$ and shear rate $\bar{\dot{\gamma}}$ are evaluated from the axial torque acting on the inner cylinder T and the angular rotation speed of the outer cylinder Ω. Gradually increasing Ω and measuring T, the apparent flow curve $\bar{\tau}(\bar{\dot{\gamma}})$ is obtained. In the numerical validation, the wide-gap rheometry was applied to a shear-thinning fluid, which obeys the power law model. The obtained apparent flow curves under different combinations of the consistency and the power law exponent are confirmed to be linear in the log-log scale graph. The evaluated power law exponents of the apparent flow curves show good correspondence with the original values, while the consistencies evaluated from the apparent flow curves are estimated lower than the original values as the degree of shear-thinning increases. This deviation can be suppressed by decreasing the radius of the outer cylinder, it is therefore important to optimize the geometry while satisfying the gap size is at least ten times larger than the dispersion size to ensure the fluid is homogeneous at that scale. In experimental aspects, three kinds of test fluids were examined; silicone oil as a Newtonian fluid, carboxymethyl cellulose (CMC) aqueous solution as a typical shear-thinning fluid, and rice porridge as spatially heterogeneous non-Newtonian fluids. The flow curves of the silicone oil and the CMC solution are confirmed to well match those evaluated by a standard torque-type rheometer. In addition, the consistency and the power law exponent of the porridge evaluated by the wide-gap torque-type rheometer also have good agreements with those obtained by the velocity-profiling-assisted rheometry. Through these numerical and experimental validations, it was reinforced that the wide-gap torque-type rheometer is a practical method to evaluate shear-rate-dependent viscosity of heterogeneous fluids, as long as the non-slip condition and the dispersion size restriction are satisfied.

acknowledgements

This work was financially supported by JSPS KAKENHI (Grant No. 22J20991), Creative Research Institution of Hokkaido University, and The Public Foundation of Elizabeth Arnold-Fuji, Japan. The authors thank technical support of Anton Paar GmbH along academic collaboration agreement. The authors would like to acknowledge the reviewers for improving the quality of this manuscript.

conflict of interest

The authors have no conflicts to disclose.

ethics approval

Ethics approval is not required.

data availability statement

The data that support the findings of this study are available from the corresponding author upon reasonable request.

references

[1] Houska M, Valentova H, Novotna P, Strohalm J, Sestak J, Pokorny J. Shear rates during oral and nonoral perception of viscosity of fluid foods. *Journal of Texture Studies* 1998;29(6):603–615.

[2] Yoshimatsu Y,Melgaard D,Westergren A, Skrubbeltrang C, Smithard DG. The diagnosis of aspiration pneumonia in older persons: a systematic review. *European Geriatric Medicine* 2022;13(5):1071–1080.

[3] Ueda A, Nohara K. Criteria for diagnosing aspiration pneumonia in Japan–A scoping review. *Respiratory Investigation* 2024;62(1):128–136.

[4] Takahashi T, Nitou T, Tayama N, Kawano A, Ogoshi H. Effects of physical properties and oral perception on transit speed and passing time of semiliquid foods from the mid-pharynx to the hypopharynx. *Journal of Texture Studies* 2002;33(6):585–598.

[5] Kumagai H, Tashiro A, Hasegawa A, Kohyama K, Kumagai H. Relationship between flowproperties of thickener solutions and their velocity through the pharynx measured by the ultrasonic pulse Doppler method. *Food Science and Technology Research* 2009;15(3):203–210.

[6] Tashiro A,Hasegawa A, Kohyama K, Kumagai H, Kumagai H. Relationship between the rheological properties of thickener solutions and their velocity through the pharynx as measured by the ultrasonic pulse Doppler method. *Bioscience, Biotechnology, and Biochemistry* 2010;74(8):1598–1605.

[7] Zhu J,Mizunuma H,Michiwaki Y. Determination of characteristic shear rate of a liquid bolus through the pharynx during swallowing. *Journal of Texture Studies* 2014;45(6):430–439.

[8] Gao Z, Kohyama K. Ultrasound PulsedWave D oppler Imaging of the Esophagus Illustrates the Effects ofWater Volume on Bolus Kinematics. *Journal of Texture Studies* 2014;45(5):335–343.

[9] Qazi WM, Ekberg O, Wiklund J, Mansoor R, Stading M. Simultaneous X-ray video-fluoroscopy and pulsed ultrasound velocimetry analyses of the pharyngeal phase of swallowing of boluses with different rheological properties. *Dysphagia* 2020;35:898–906.

[10] Nishinari K, Takemasa M, Su L, Michiwaki Y, Mizunuma H, Ogoshi H. Effect of shear thinning on aspiration–Toward making solutions for judging the risk of aspiration. *Food Hydrocolloids* 2011;25(7):1737–1743.

[11] Vickers Z, Damodhar H, Grummer C, Mendenhall H, Banaszynski K, Hartel R, et al. Relationships among rheological, sensory texture, and swallowing pressure measurements of hydrocolloid-thickened fluids. *Dysphagia* 2015;30:702–713.

[12] Hadde E, Chen J. Shear and extensional rheological characterization of thickened fluid for dysphagia management. *Journal of Food Engineering* 2019;245:18–23.

[13] Nishinari K, Turcanu M, Nakauma M, Fang Y. Role of fluid cohesiveness in safe swallowing. *npj Science of Food* 2019;3(1):5.

[14] Ross AI, Tyler P, Borgognone MG, Eriksen BM. Relationships between shear rheology and sensory attributes of hydrocolloid-thickened fluids designed to compensate for impairments in oral manipulation and swallowing. *Journal of Food Engineering* 2019;263:123–131.

[15] Tobin AB, Mihnea M, Hildenbrand M, Miljkovic A, Garrido-Bañuelos G, Xanthakis E, et al. Bolus rheology and ease of swallowing of particulated semi-solid foods as evaluated by an elderly panel. *Food & Function* 2020;11(10):8648–8658.

[16] Irgens F. Rheology and non-newtonian fluids. *Springer*; 2014.

[17] Barnes HA. A review of the slip (wall depletion) of polymer solutions, emulsions and particle suspensions in viscometers: its cause, character, and cure. *Journal of Non-Newtonian Fluid Mechanics* 1995;56(3):221–251.

[18] Barnes HA. Measuring the viscosity of large-particle (and flocculated) suspensions—a note on the necessary gap size of rotational viscometers. *Journal of Non-Newtonian Fluid Mechanics* 2000;94(2-3):213–217.

[19] Ohie K, Nishizuka D, Yoshida T, Tasaka Y. Cost-effective production of density-controllable monodisperse spheres for experiments in fluids. *Physics of Fluids* 2024;36(9).

[20] Yoshida T, Tasaka Y, Fischer P. Ultrasonic spinning rheometry test on the rheology of gelled

food for making better tasting desserts. *Physics of Fluids* 2019;31(11).
[21] Ohie K, Yoshida T, Tasaka Y. Coupling a torque rheometer with an ultrasonic velocity profiler for evaluating multiphase fluids in oscillatory shear flows. *Journal of Rheology* 2024;68(5):665–678.
[22] Schatzmann M, Fischer P, Bezzola GR. Rheological behavior of fine and large particle suspensions. *Journal of Hydraulic Engineering* 2003;129(10):796–803.
[23] Schatzmann M, Bezzola GR, Minor HE, Windhab EJ, Fischer P. Rheometry for large-particulated fluids: analysis of the ball measuring system and comparison to debris flow rheometry. *Rheologica Acta* 2009;48:715–733.
[24] Asai K, Ichiyanagi M, Satone H, Mori T, Tsubaki J, Itoh Y. The influence of mon-Newtonian property on the apparent viscosity measured by single cylinder rotational viscometer (type-B viscometer). *Journal of the Society of Powder Technology*, Japan 2009;46(12):873–880.
[25] Tsetsekou A, Agrafiotis C,Milias A. Optimization of the rheological properties of alumina slurries for ceramic processing applications Part I: Slip-casting. *Journal of the European Ceramic Society* 2001;21(3):363–373.
[26] Tsetsekou A, Agrafiotis C, Leon I, Milias A. Optimization of the rheological properties of alumina slurries for ceramic processing applications Part II: Spray-drying. *Journal of the European Ceramic Society* 2001;21(4):493–506.
[27] Stokes GG, et al. On the effect of the internal friction of fluids on the motion of pendulums 1851.
[28] Batchelor GK. An introduction to fluid dynamics. Cambridge university press; 1967.
[29] Murai Y, Oiwa H. Increase of effective viscosity in bubbly liquids from transient bubble deformation. *Fluid Dynamics Research* 2008;40(7-8):565.
[30] LiW, Iwama T, Yu H, Ueda S, Saito N, Inoue R. Apparent viscosity measurement of solid-liquid coexisting fluid by falling ball method for evaluation iron particle sedimentation velocity in slag. *ISIJ International* 2021;61(12):2915–2922.
[31] Mori T, Moriyama S, Nakagawa T, Tsubaki J. Measurement of apparent viscosity of various fluids by using B-type and vibration-type viscometers. *Nihon Reoroji Gakkaishi* 2017;45(4):157–165.
[32] Mischenko S, Mordasov M, Savenkov A, Sychev V. Analysis of the influence of sizes of a vessel with a liquid on the readings of Brookfield viscometer. *Measurement Techniques* 2020;63:288–294.
[33] Salmon JB, Bécu L,Manneville S, Colin A. Towards local rheology of emulsions under Couette flow using Dynamic Light Scattering. *The European Physical Journal E* 2003;10:209–221.
[34] Bécu L, Manneville S, Colin A. Yielding and flow in adhesive and nonadhesive concentrated emulsions. *Physical Review Letters* 2006;96(13):138302.
[35] Divoux T, Tamarii D, Barentin C, Teitel S, Manneville S. Yielding dynamics of a Herschel–Bulkley fluid: a critical-like fluidization behaviour. *Soft Matter* 2012;8(15):4151–4164.
[36] Derakhshandeh B, Vlassopoulos D, Hatzikiriakos SG. Thixotropy, yielding and ultrasonic Doppler velocimetry in pulp fibre suspensions. *Rheologica Acta* 2012;51:201–214.
[37] Gallot T, Perge C, Grenard V, Fardin MA, Taberlet N, Manneville S. Ultrafast ultrasonic imaging coupled to rheometry: Principle and illustration. *Review of Scientific Instruments* 2013;84(4).
[38] Takeda Y. Velocity profile measurement by ultrasonic Doppler method. *Experimental Thermal and Fluid Science* 1995;10(4):444–453.
[39] Takeda Y. Ultrasonic Doppler velocity profiler for fluid flow, *Springer Science & Business Media*; 2012.
[40] Tan C, Murai Y, LiuW, Tasaka Y, Dong F, Takeda Y. Ultrasonic Doppler technique for application to multiphase flows: A review. *International Journal of Multiphase Flow* 2021;144:103811.
[41] Ohie K, Yoshida T, Tasaka Y, Murai Y. Flow prediction of complex fluids in a circular pipe by utilizing a velocity-profiling-assisted rheometer. *Industrial & Engineering Chemistry Research* 2022;61(49):18157–18164.

[42] Ohie K, Kumagai S, Tasaka Y, Murai Y. Rheology of fluid foods containing millimeter-sized ingredients examined by velocity-profiling-assisted rheometry and prediction of spreading and descending behaviors. *Journal of Rheology* 2025; 69(2):111−120.
[43] Noto D, Ohie K, Yoshida T, Tasaka Y. Optical spinning rheometry test on viscosity curves of less viscous fluids at low shear rate range. *Experiments in Fluids* 2023;64(1):18.
[44] Tasaka Y, Kimura T,Murai Y. Estimating the effective viscosity of bubble suspensions in oscillatory shear flows by means of ultrasonic spinning rheometry. *Experiments in Fluids* 2015;56(1):1867.
[45] Batchelor, GK, An introduction to fluid dynamics. *Cambridge university press* 2000.
[46] Wilkinson WL, Non-Newtonian fluids. *Pergamon Press, Oxford* 1960.
[47] Ouriev B and Windhab EJ. Rheological study of concentrated suspensions in pressure-driven shear flow using a novel in-line ultrasound Doppler method. *Experiments in Fluids* 2002; 32(2):204−211.
[48] Ghannam MT, Esmail MN. Rheological properties of carboxymethyl cellulose. *Journal of Applied Polymer Science* 1997;64(2):289–301.
[49] Benchabane A, Bekkour K. Rheological properties of carboxymethyl cellulose (CMC) solutions. *Colloid and Polymer Science* 2008;286(10):1173–1180.
[50] Ohie K, Chiba H, Kumagai S, Yoshida T, Tasaka Y. A method for evaluating time-resolved rheological functionalities of fluid foods. *Journal of Texture Studies* 2022;53(4):444−452.
[51] Djalili-Moghaddam M, Toll S. Fibre suspension rheology: effect of concentration, aspect ratio and fibre size. *Rheologica Acta* 2006;45:315−320.
[52] Marín-Santibáñez BM, Pérez-González J, de Vargas L. Shear rheometry and visualization of glass fiber suspensions. *Rheologica Acta* 2010;49:177−189.